Title: Parvalbumin interneurons mediate neuronal circuitry-neurogenesis coupling in the adult hippocampus.
Authors: Song J, Sun J, Moss J, Wen Z, Sun GJ, Hsu D, Zhong C, Davoudi H, Christian KM, Toni N, Ming GL, Song H
Journal: Nature neuroscience
Year: 2013 Dec
Volume: 16
Issue: 12
Pages: 1728-30
DOI: 10.1038/nn.3572

Published in final edited form as:
Nat Neurosci. 2013 December ; 16(12): 1728–1730. doi:10.1038/nn.3572.

Parvalbumin interneurons mediate neuronal circuitry-neurogenesis coupling in the adult hippocampus

Juan Song[1,2], **Jiaqi Sun**[1,3,*], **Jonathan Moss**[4,*], **Zhexing Wen**[1,2,*], **Gerald J. Sun**[1,5], **Derek Hsu**[1], **Chun Zhong**[1,2], **Heydar Davoudi**[1], **Kimberly M. Christian**[1,2], **Nicolas Toni**[4,#], **Guo-li Ming**[1,2,5,#], and **Hongjun Song**[1,2,5,#]

[1]Institute for Cell Engineering, Johns Hopkins University School of Medicine, Baltimore, MD 21205, USA. [2]Department of Neurology, Johns Hopkins University School of Medicine, Baltimore, MD 21205, USA. [3]School of Life Sciences, Tsinghua University, Beijing 100084, P.R. China. [4]Department of Fundamental Neurosciences, University of Lausanne, 9 Rue du Bugnon, 1005 Lausanne, Switzerland. [5]The Solomon H. Snyder Department of Neuroscience, Johns Hopkins University School of Medicine, Baltimore, MD 21205, USA.

Abstract

Using immunohistology, electron microscopy, electrophysiology and optogenetics, we show that proliferating adult hippocampal neural precursors receive immature GABAergic synaptic inputs from parvalbumin-expressing interneurons. Recently shown to suppress quiescent neural stem cell activation, parvalbumin interneuron activation promotes newborn neuronal progeny survival and development. Our study suggests a niche mechanism involving parvalbumin interneurons that couples local circuit activity to diametric regulation of two critical initial phases of adult hippocampal neurogenesis.

One fundamental question in stem cell biology is whether and how niche factors couple tissue demands to produce proper numbers of progeny from somatic stem cells. In the adult subgranular zone (SGZ), a substantial loss of newborn progeny occurs during the first 4 days after they are born[1–4]. Adult hippocampal neurogenesis occurs within a dynamic neuronal network; therefore we hypothesized that the local circuit activity may serve as an effective indicator of current tissue demands and provide a signal to regulate this critical event.

We used retroviruses expressing GFP to birth-date proliferating neural progenitors in the adult SGZ[5]. At 4 days post viral injection (dpi), 92% of GFP^+ cells were $MCM2^+$ and 81% were DCX^+MCM2^+ proliferating neuroblasts (Supplementary Fig. 1). Whole-cell recordings in acute slices showed that 95% of GFP^+ cells recorded responded to GABA (n = 37; Supplementary Fig. 2a). Confocal imaging analysis revealed close association of GFP^+ cells with $synapsin^+GAD67^+$ GABAergic presynaptic boutons (Supplementary Fig. 2b and

Correspondence should be addressed to: Hongjun Song, Ph.D., Institute for Cell Engineering, Department of Neurology, Johns Hopkins University School of Medicine, 733 N. Broadway, MRB 759, Baltimore, MD 21205, USA. Tel: 443-287-7499; Fax: 410-614-9568; shongju1@jhmi.edu.
*, #These authors contribute equally to this work.

COMPETINGNG FINANCNCIAL INTERESTS: The authors declare no competing financial interests.

Supplementary Movie 1). As previously shown[6, 7], presynaptic terminals onto newborn progeny were observed by immuno-electron microscopy (immuno-EM; Fig. 1a). While none of GFP^+ cells recorded (n = 55) exhibited any spontaneous, or evoked post-synaptic currents (PSCs) in response to 0.1 Hz field stimulation (Supplementary Fig. 2c), bicuculline-sensitive PSCs were recorded in 14.3% of GFP^+ cells upon 5 Hz stimulation (n = 35; Supplementary Fig. 2d), suggesting an immature nature of these synapses. This result is in contrast to that has been observed in the adult subventricular zone, where neuroblasts are activated by tonic, but not synapitc GABA[8].

We next explored the sources of GABAergic inputs. Confocal and light microscopy analyses revealed close associations of parvalbumin-expressing (PV^+) $synapsin^+$ puncta with GFP^+ cells at 4 dpi (Fig. 1b and Supplementary Movie 2), including those that were proliferating ($MCM2^+$; Supplementary Fig. 3). Immuno-EM showed symmetric synaptic contacts between vesicle-filled PV^+ axonal terminals and newborn progeny (Figs. 1c-d and Supplementary Figs. 4a-f), which were very similar to those between PV^+ neurons and unlabelled mature neurons (Fig. 1e and Supplementary Figs. 4m-p). Interestingly, various contacts exist between PV^+ axons and newborn progeny, ranging from proximal PV^+ boutons to mature-looking symmetric synapses (Supplementary Figs. 4a-l).

To determine whether observed synaptic structures are functional, we selectively expressed ChR2-YFP in dentate PV^+ neurons using adult *PV-Cre* mice[9] and labelled proliferating neural progenitors with RFP (Supplementary Fig. 5). Light stimulation at 8 Hz, but not 0.1 Hz, led to GABAergic PSCs in 17% of RFP^+ cells examined at 4 dpi in acute slices (n = 48; Fig. 1f). The low induction rate, small amplitude and broad distribution of rise times of evoked PSCs recorded in RFP^+ cells reflect characteristics of immature synapses (Figs. 1g-i). Importantly, blockade of glutamatergic synaptic transmission had no effect on PSCs recorded (Figs. 1g-h), supporting the presence of monosynaptic connections from PV^+ neurons. Interestingly, optogenetic activation of somatostatin-expressing (SST^+) interneurons led to evoked PSCs in mature dentate granule neurons, but not in RFP^+ cells (Fig. 1g).

The identification of PV^+ neurons as one source of synaptic inputs onto newborn progeny, although not eliminating the possibility of inputs from other neurons[7, 10], provided an entry point to investigate how local circuitry may regulate these progeny *in vivo*. We labelled proliferating neural progenitors with EdU and then applied light-induced activation of $ChR2^+PV^+$ interneurons between 1 and 4 dpi (Fig. 2a). Consistent with previous findings[1–4], stereological quantification in the no-light sham group showed a significant decrease of EdU^+ cells in the adult SGZ from 1 to 4 dpi (Figs. 2b-c). Interestingly, 8 Hz light stimulation led to significant increases of EdU^+ cells and EdU^+DCX^+ neuronal progeny at 4 dpi compared to the sham no-light treatment (Figs. 2c-d). The survival effect was accompanied by reduction of dying cells, identified by pyknotic nuclei surrounded by $Iba\text{-}1^+$ microglia (Figs. 2e-g), as previously reported[1]. NeuroD has been suggested to promote newborn neuron survival during adult SGZ neurogenesis[11, 12]. Indeed, there was a significant increase of $EdU^+NeuroD^+$ cells upon light stimulation (Supplementary Fig. 6a). In contrast, percentages of EdU^+ cells that remained in cell cycle ($MCM2^+$) or underwent neuronal differentiation (DCX^+) were not significantly different (Supplementary Figs. 6b-c).

Importantly, similar optogenetic manipulation of dentate SST^+ interneurons had no effect (Figs. 2c-d and Supplementary Figs. 6b-c).

To assess the role of endogenous PV^+ neuron activity for newborn progeny survival, we selectively expressed NpHR in dentate PV^+ neurons and optogenetically suppressed $NpHR^+PV^+$ neurons between 1 and 4 dpi (Supplementary Figs. 7a-c). Stereological quantification showed a further decrease in EdU^+MCM2^+ proliferating neural precursors and DCX^+EdU^+ neuronal progeny from 1 to 4 dpi (Figs. 3a-b). The number of dying cells surrounded by Iba-1^+ microglia was increased (Figs. 3c-d), whereas that of $EdU^+NeuroD^+$ progeny was decreased (Supplementary Fig. 7h). No significant difference was found for cell cycle exit or neuronal differentiation of EdU^+ cells (Supplementary Figs. 7d-e). An independent approach to suppress PV^+ neuron activity using Arch showed similar effects as NpHR, while SST^+ neuron suppression had no effect (Figs. 3a-b and Supplementary Figs. 7d-e).

Loss of proliferating precursors could have a bigger impact on the ultimate number of mature adult-born neurons than the loss of individual post-mitotic neurons (Fig. 3e). Indeed, PV^+ neuron suppression between 1 to 4 dpi led to an 18.9% decrease of EdU^+MCM2^+ proliferating neural progeny at 4 dpi, but a 49% decrease of EdU^+NeuN^+ neurons at 30 dpi (Figs. 3e-f).

Adult neurogenesis is dynamically regulated by external stimuli[13]. We introduced mice to an enriched environment between 1 and 4 dpi, an experience known to increase PV^+ neuron activity[14]. This treatment significantly increased EdU^+, EdU^+DCX^+ and $EdU^+NeuroD^+$ progeny at 4 dpi compared to animals in standard conditions (Figs. 3g-h and Supplementary Fig. 7h). Remarkably, PV^+ neuron suppression largely abolished the survival effect of an enriched environment (Fig. 3h). Thus, PV^+ neuron activity is also involved in experience-dependent regulation of early critical phases of adult hippocampal neurogenesis.

Finally, we examined whether PV^+ neuron activity continues to influence neuronal progeny beyond 4 dpi. Indeed, PV^+ neuron-induced synaptic activation was detected at 7 dpi (Supplementary Fig. 8a). Interestingly, optogenetic activation of PV^+ neurons between 4 and 7 dpi promoted dendritic development of newborn neurons, whereas suppression of PV^+ neuron activity resulted in the opposite effect (Supplementary Figs. 8b-f).

We identified a novel neuronal circuitry-based niche mechanism regulating proliferating neuronal progeny survival and their development via local PV^+ interneuron activity. While PV^+ neurons make direct synaptic contacts with these newborn progeny, the optogenetic approach used here does not rule out potential contributions from secondary circuitry modulation, nor factors other than GABA. In sharp contrast to the increased survival of newborn progeny, PV^+ neuron activation, via nonsynaptic GABAergic signalling, inhibits quiescent neural stem cell activation[9]. Together, these results reveal a striking diametric regulation of two early critical steps of adult neurogenesis via PV^+ neuron activity (Supplementary Fig. 9a). Computational models have suggested advantages of circuit activity-neurogenesis coupling for temporal storage and memory clearing in the adult hippocampus[15, 16]. Experimental evidence also suggests that a proper rate of both addition

and elimination of new neurons optimizes behavioural outcomes in animal models[17, 18]. What are potential advantages of such a diametric mode of neuronal circuitry-neurogenesis coupling? First, it promotes an adaptive regulation of adult neurogenesis – a lack of dentate neuronal activity minimizes the need to retain and develop new neurons that were just born, but increases the quiescent neural stem cell pool via symmetric cell division to prepare for the future. Second, it facilitates time-stamping of a specific cohort of newborn neurons during a period of heightened dentate activity by increasing their survival while simultaneously suppressing upcoming generation of new neurons from neural stem cell activation. This could be particularly important, given recent behavioural studies suggesting a critical contribution of newborn neurons at specific developmental stages to hippocampal function[13, 19]. Our findings point to the presence of multiple critical periods in regulating progeny survival via circuit-based, activity-dependent mechanisms[20] (Supplementary Fig. 9b), which may facilitate the development of novel strategies to enhance functional repair from endogenous or transplanted neurons after injury and degenerative neurological disorders.

ONLINE METHODS

Construction, production and stereotaxic injection of engineered retroviruses and AAV

Engineered murine oncoretroviruses expressing GFP or RFP were used to birth-date and label proliferating cells and their progeny as previously described[5, 21, 22]. For experiments without optogenetic manipulations, adult mice (8 weeks old, female, C57BL/6 background; Charles River) housed under the standard condition or enriched environment[23] were anaesthetized and retroviruses were stereotaxically injected into the dentate gyrus at 2 sites as previously described[5, 22]. Immunohistological or electrophysiological analysis was performed at 2–10 dpi as previously described[5, 22].

Cre-dependent recombinant AAV vectors were used for cell type-specific transgene expression[24–26]. AAV vectors were obtained from vector cores of University of Pennsylvania and University of North Carolina. Transgenic *PV-Cre* (B6;129P2-*Pvalb*$^{tm1(cre)Arbr}$/J) and *SST-Cre* (mixed background, *Sst*$^{tm21(cre)Zjh}$/J) mice were obtained from the Jackson Laboratory. Stereotaxic injection of AAV was performed using following coordinates: anterioposterior = − 2 mm from Bregma; lateral = ± 1.5 mm; ventral = 2.2 mm. For the cell survival assay, optic fibers (Doric Lenses, Inc) were implanted at same injection sites right after AAV injection with a depth of 1.6 mm from the skull surface. Animals were then allowed to recover for 4 weeks before analyses. The specificity and efficacy of expression of opsins in PV^+ and SST^+ neurons have been previously characterized[9]. All animal procedures were performed in accordance with institutional guidelines.

In vivo optogenetic manipulation, immunostaining, confocal imaging, processing and quantification

For analysis of neurogenesis after optogenetic and environmental manipulation[23], adult *PV-Cre* or *SST-Cre* mice at 4 weeks after AAV injection were pulsed with EdU (32.5 mM EdU stock solution, 41.1 mg/kg body weight, *i.p.*) four times with the interval of 2.5 hr. Twenty-four hours after the first EdU injection, the *in vivo* light paradigm was administered as

previously described[9]. For ChR2 stimulation, blue light flashes (472 nm) lasting 5 ms at 8 Hz programmed by Master 8 through DPSSL laser system (Laser century Co. Ltd., Shanghai, China) were delivered *in vivo* every 5 min for 30 s/per trial. For eNpHR or Arch stimulation, continuous yellow light (593 nm) was delivered *in vivo*. For opsin stimulation, the whole light stimulation paradigm lasted 8 hr per day for 4 consecutive days (Fig. 2a and Supplementary Fig. 7a). At the end of the 4th day, animals were processed for immunohistology. Given the expected light spread *in vivo*, every 6th section within a distance 1.0 mm anterior and posterior to injection sites were used for quantification and analysis. Histological and electrophysiological analyses showed that these treatments did not lead to defects in the structural integrity of the dentate gyrus, significant cell death, or changes of PV$^+$ neuron properties in the adult dentate gyrus and no obvious behavioural differences were observed[9] (and data not shown).

For immunohistology, coronal brain sections (40 μm in thickness) were processed as previously described[5]. EdU labelling was processed using Click-iT® EdU Alexa Fluor imaging kit (Invitrogen). The following primary antibodies were used: Tbr2 (Abcam; rabbit; 1:1000), DCX (Santa Cruz; Goat; 1:500), MCM2 (BD; mouse; 1:500), PV (Swant; mouse, rabbit or goat; 1:500), SST (Millipore; rat; 1:200), synapsin I (Molecular Probes; rabbit; 1:500), GAD67 (Chemicon; mouse or rabbit; 1:500), Iba-1 (Millipore; rabbit; 1:500); NeuN (Millipore; mouse; 1:500), and NeuroD (Santa Cruz; goat; 1:250). Images were acquired on a Zeiss LSM 710 multiphoton confocal system (Carl Zeiss, Thornwood, NY, USA) using a multi-track configuration. Stereological quantification was assessed in the adult SGZ using a modified optical fractionator technique as previously described[27]. For dendritic analysis, 3D reconstruction of entire dendritic processes of each newborn neuron at 10 dpi was made from Z-series stacks of confocal images. The 2D projection images were traced with NIH ImageJ. All newborn dentate granule neurons with largely intact dendritic trees were analyzed for total dendritic length as described[5, 28]. The measurements did not include corrections for inclinations of dendritic process and therefore represented projected lengths. Sholl analysis for dendritic complexity was carried out by counting the number of dendrites that crossed a series of concentric circles at 10 μm intervals from the soma as previously described[28]. All quantifications were performed by investigators blind to experimental conditions.

Electron microscopy analyses

Adult *PV-Cre* mice were stereotaxically injected with DIO-GFP AAV and followed by injection of retroviruses expressing GFP four weeks later. Four days after retroviral injection, mouse brains were processed for immuno-EM as previously described[29, 30]. Briefly, mice were transcardially perfused with 4% PFA in 0.1 M phosphate buffer saline (PBS), pH 7.4, and maintained at 4°C. Brains were removed 15 hr after the perfusion and post-fixed for 72 hr in 4% PFA in 0.1 M PBS. Coronal sections (50 μm in thickness) were then sectioned using a vibratome and observed with an epifluorescence microscope. Sections containing clearly-labelled newborn progeny and PV$^+$ terminals were cryoprotected in 2% glycerol and 20% DMSO (vol/vol) in 0.1 M PBS for 20 min and freeze-thawed four times in liquid nitrogen. After a treatment in 0.3% hydrogen peroxide in 0.1 M PBS (vol/vol, five times for 5 min) and three 10 min washes in 0.5% bovine serum albumin in 0.1 M PBS

(vol/vol, BSA-C, Aurion), sections were incubated overnight in the primary antibody (rabbit anti-GFP, Chemicon, 1:500 in 0.1% BSA-C in 0.1 M PBS, 40 hr at 4°C on a shaker). After washing in 0.1% BSA-C in 0.1 M PBS, the sections were incubated for 5 hr at 20 ± 5°C in biotinylated secondary antibody (goat anti-rabbit, F_{ab} fragment, Jackson Laboratories, 1:200, 0.1% BSA-C in 0.1 M PBS). Sections were incubated for 2 hr in avidin biotin peroxidase complex (ABC Elite, Vector Laboratories), followed by a reaction with 3,3-diaminobenzidine (Vector Laboratories Kit, 10–20 min). The sections were then post-fixed overnight in 2.5% glutaraldehyde in 0.1 M PB buffer (wt/vol), washed in 0.1 M PBS, post-fixed in osmium tetroxide for 1 hr, dehydrated in ascending concentrations of ethanol and then acetone, and embedded in Epoxy resin. Locations of clearly-labelled newborn progeny and PV^+ terminals were identified at the light microscopic level (Supplementary Fig. 4a, m) and followed through to the electron microscopic level. Serial sections (60 nm in thickness) were collected on single-slot copper grids and contrasted by incubating for 35 min in 5% uranyl acetate solution in dH_2O (wt/vol) and then 25 min in a Reynolds solution. Sections were then examined using a Philips CM10 transmission electron microscope and serial images of the labelled structures were captured using a digital camera (Morada SIS, Olympus). These images were then aligned and 3D structures were rendered using Fiji and 3D Studio Max software (Figs. 1a, c, e and Supplementary Fig. 4f).

Electrophysiology analysis

Adult mice housed under standard conditions were processed at 3–7 dpi for slice preparation as previously described[5, 9, 22]. The brains were quickly removed into the ice-cold solution (in mM: 110 choline chloride, 2.5 KCl, 1.3 KH_2PO_4, 25.0 $NaHCO_3$, 0.5 $CaCl_2$, 7 $MgSO_4$, 20 dextrose, 1.3 sodium L-ascorbate, 0.6 sodium pyruvate, 5.0 kynurenic acid). Slices (275 μm in thickness) were cut using a vibrotome (Leica VT1000S) and transferred to a chamber containing the external solution (in mM: 125.0 NaCl, 2.5 KCl, 1.3 KH_2PO_4, 1.3 $MgSO_4$, 25.0 $NaHCO_3$, 2 or 5 $CaCl_2$, 1.3 sodium L-ascorbate, 0.6 sodium pyruvate, 10 dextrose, pH 7.4, 320 mOsm), bubbled with 95% O_2/5% CO_2. Electrophysiological recordings were obtained at 32–34°C. GFP^+ or RFP^+ cells within the SGZ were visualized by DIC and fluorescence microscopy. Mature granule cells in the outer granule cell layer in the same slices were recorded for comparison. The whole-cell patch-clamp configuration was employed in the voltage-clamp mode (V_m = −65 mV). Microelectrodes (4–6 MΩ) were pulled from borosilicate glass capillaries and filled with the internal solution containing (in mM): 135 CsCl gluconate, 15 KCl, 4 $MgCl_2$, 0.1 EGTA, 10.0 HEPES, 4 ATP (magnesium salt), 0.3 GTP (sodium salt), 7 phosphocreatine (pH 7.4, 300 mOsm). Additional chemicals were used at the following final concentrations in the bath as indicated: bicuculline (50–100 μM), CNQX (20 μM) and AP5 (50 μM). All chemicals were purchased from Sigma except bicuculline (Tocris). Data were collected using an Axon 200B amplifier and acquired with a DigiData 1322A (Axon Instruments) at 10 kHz. For measuring GABA-induced responses from GFP^+ cells, focal pressure ejection of 10 μM GABA through a puffer pipette controlled by a Picospritzer (5 ms puff at 3–5 psi) was used to activate $GABA_A$Rs. A bipolar electrode (World Precision Instruments) was used to stimulate (0.1 ms duration) the dentate granule cell layer. Low frequency (0.1 Hz) and theta bursts (5 Hz, 10 s duration) were delivered to stimulate the granule cell layer in the presence or absence of bicuculline (100 μM). The stimulus intensity (50 μA) was maintained for all experiments.

For experiments with light stimulation of PV^+ or SST^+ neurons, retroviruses expressing RFP were stereotaxically delivered to the adult dentate gyrus to label proliferating neural progenitors at 4 weeks after AAV injection. Electrophysiology recordings were performed 4 days after retroviral injection. To stimulate ChR2 in PV^+ or SST^+ neurons, light flashes (0.1 or 8 Hz) generated by a Lambda DG-4 plus high speed optical switch with a 300W Xenon lamp and a 472 nm filter set (Chroma) were delivered to coronal sections through a 40X objective (Carl Zeiss). To stimulate eNpHR or Arch in PV^+ neurons, continuous yellow light generated by DG-4 plus system with a 593 nm filter set was delivered to coronal sections through a 40X objective as previously described[9].

Statistical analysis

Statistical analysis was performed with one-way ANOVA (with Tukey *post hoc* test), two-tailed unpaired Student's t-test, or two sample Kolmogorov–Smirnov test, as indicated in the text and figures. When a significant interaction was found upon performing two-way ANOVA, simple main effects were determined by a two-tailed unpaired Student's t-test. Validation of normality and homogeneity of variance assumptions was performed for all compared data groups using Shapiro-Wilk and Levene's tests, respectively. All statistical analyses were performed using Origin software (OriginLab) or Matlab (Mathworks).

Supplementary Material

Refer to Web version on PubMed Central for supplementary material.

Acknowledgments

We thank members of Song and Ming laboratories for discussion, L. Tsai and K. Deisseroth for initial help with optogenetics, and Q. Hussaini, Y. Cai and L. Liu for technical support. This work was supported by NIH (NS047344, ES021957) and NARSAD to H.S., NIH (NS048271, HD069184), Dr. Miriam and Sheldon G. Adelson Medical Research Foundation, NARSAD, and MSCRF to G.L.M., the Swiss National Science Foundation (PP00A-119026/1) to N.T., NARSAD and MSCRF to K.M.C., and by postdoctoral fellowships from MSCRF to J.S., Z.W., and C.Z., and from the Fondation Leenaards to J.M.

REFERENCES

1. Sierra A, et al. Cell Stem Cell. 2010; 7:483–495. [PubMed: 20887954]
2. Snyder JS, et al. J Neurosci. 2009; 29:14484–14495. [PubMed: 19923282]
3. Kronenberg G, et al. J Comp Neurol. 2003; 467:455–463. [PubMed: 14624480]
4. Mandyam CD, Harburg GC, Eisch AJ. Neuroscience. 2007; 146:108–122. [PubMed: 17307295]
5. Ge S, et al. Nature. 2006; 439:589–593. [PubMed: 16341203]
6. Kaplan MS, Bell DH. J Neurosci. 1984; 4:1429–1441. [PubMed: 6726341]
7. Tozuka Y, Fukuda S, Namba T, Seki T, Hisatsune T. Neuron. 2005; 47:803–815. [PubMed: 16157276]
8. Liu X, Wang Q, Haydar TF, Bordey A. Nat Neurosci. 2005; 8:1179–1187. [PubMed: 16116450]
9. Song J, et al. Nature. 2012; 489:150–154. [PubMed: 22842902]
10. Markwardt SJ, Dieni CV, Wadiche JI, Overstreet-Wadiche L. Nat Neurosci. 2011; 14:1407–1409. [PubMed: 21983681]
11. Gao Z, et al. Nat Neurosci. 2009; 12:1090–1092. [PubMed: 19701197]
12. Kuwabara T, et al. Nat Neurosci. 2009; 12:1097–1105. [PubMed: 19701198]
13. Ming GL, Song H. Neuron. 2011; 70:687–702. [PubMed: 21609825]

14. Mann EO, Paulsen O. Trends Neurosci. 2007; 30:343–349. [PubMed: 17532059]
15. Deisseroth K, et al. Neuron. 2004; 42:535–552. [PubMed: 15157417]
16. Chambers RA, Potenza MN, Hoffman RE, Miranker W. Neuropsychopharmacology. 2004; 29:747–758. [PubMed: 14702022]
17. Kim WR, et al. Eur J Neurosci. 2009; 29:1408–1421. [PubMed: 19519627]
18. Sahay A, et al. Nature. 2011; 472:466–470. [PubMed: 21460835]
19. Gu Y, et al. Nat Neurosci. 2013; 15:1700–1706. [PubMed: 23143513]
20. Tashiro A, Sandler VM, Toni N, Zhao C, Gage FH. Nature. 2006; 442:929–933. [PubMed: 16906136]
21. van Praag H, et al. Nature. 2002; 415:1030–1034. [PubMed: 11875571]
22. Ge S, Yang CH, Hsu KS, Ming GL, Song H. Neuron. 2007; 54:559–566. [PubMed: 17521569]
23. Kempermann G, Kuhn HG, Gage FH. Nature. 1997; 386:493–495. [PubMed: 9087407]
24. Atasoy D, Aponte Y, Su HH, Sternson SM. J Neurosci. 2008; 28:7025–7030. [PubMed: 18614669]
25. Sohal VS, Zhang F, Yizhar O, Deisseroth K. Nature. 2009; 459:698–702. [PubMed: 19396159]
26. Cardin JA, et al. Nature. 2009; 459:663–667. [PubMed: 19396156]
27. Kim JY, et al. Neuron. 2009; 63:761–773. [PubMed: 19778506]
28. Duan X, et al. Cell. 2007; 130:1146–1158. [PubMed: 17825401]
29. Toni N, et al. Nat Neurosci. 2008; 11:901–907. [PubMed: 18622400]
30. Toni N, et al. Nat Neurosci. 2007; 10:727–734. [PubMed: 17486101]

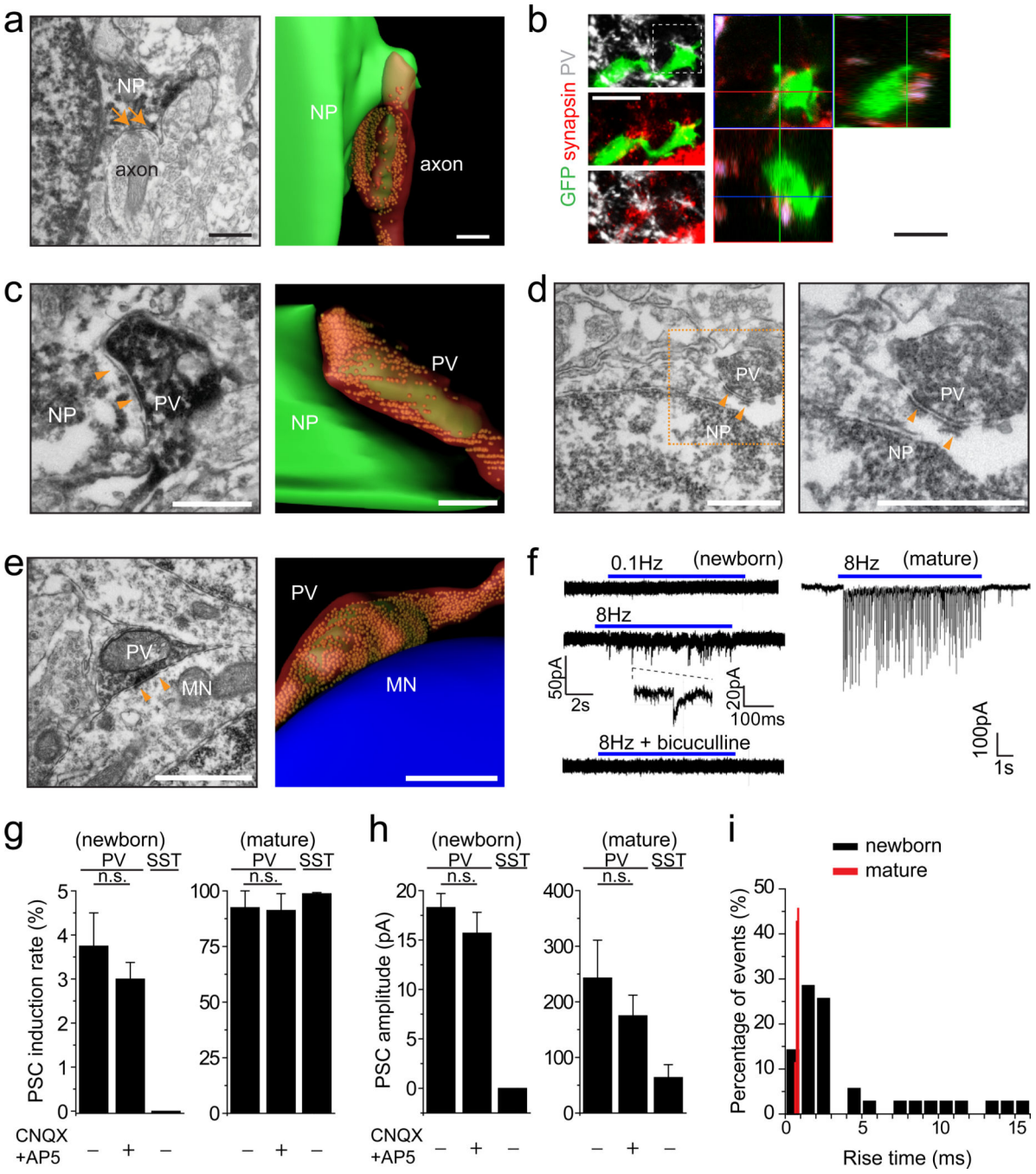

Figure 1.

PV^{+} interneurons form immature synaptic inputs onto proliferating newborn progeny in the adult dentate gyrus. (**a**) Sample immuno-EM image of a symmetrical synaptic contact (arrows) with a dark labelled newborn progeny (NP; left; Scale bar: 0.2 μm) and the serial reconstruction (right; Scale bar: 0.8 μm). (**b**) Sample confocal images of immunostaining for PV, synapsin I, and GFP (left) with orthogonal views (right). Scale bars: 20 μm. See Supplementary Movie 1 for 3D reconstruction and Supplementary Fig. 3 for another example for a proliferating newborn progeny. (**c-e**) Sample images and serial

reconstructions of symmetrical synaptic contacts (arrowheads) between vesicle-filled PV^+ axon terminals and newborn progeny (NP; **c, d**) or unlabelled mature neurons (MN; **e**). Please see Supplementary Fig. 4 for correlative light and EM analyses for the identification of labelled PV^+ axonal terminals, labelled newborn progeny and unlabeled mature granule cell shown in (**c, e**). Scale bars: 1 μm. (**f**) Sample traces of whole-cell voltage-clamp recording of a RFP^+ new progeny and a mature granule cell in the same preparation upon light stimulation (472 nm; 5 ms) of ChR2-expressing PV^+ neurons. (**g-i**) Summaries of induction rate (**g**), mean amplitude (**h**), and distribution of rise times (**i**) of evoked PSC recorded from RFP^+ newborn progeny at 4 dpi and from mature granule neurons upon 8 Hz light stimulation of ChR2-expressing PV^+ or SST^+ neurons. Values represent mean ± s.e.m. (n = 3–8 cells; n.s.: $P > 0.1$; Student's t-test).

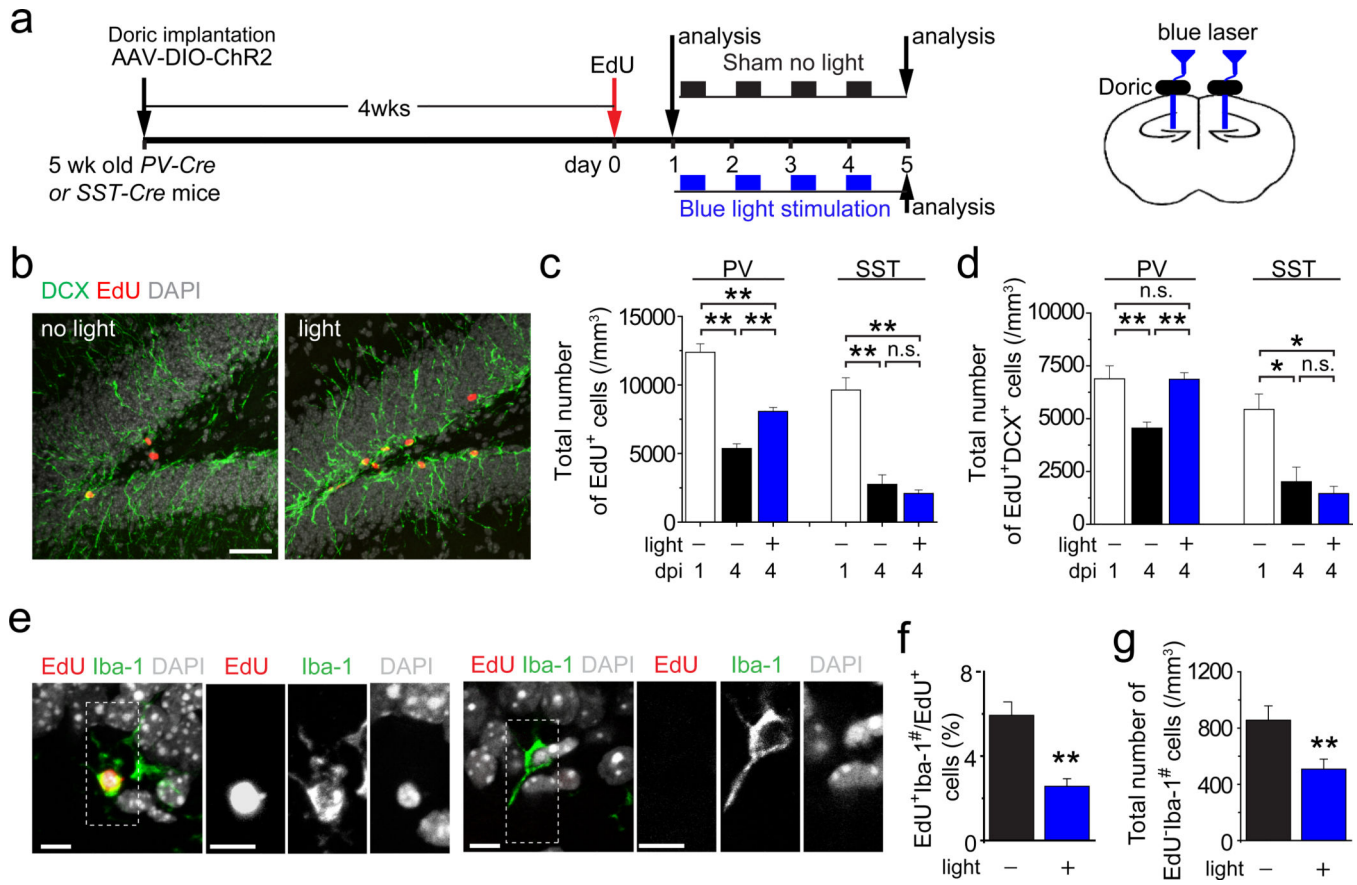

Figure 2.

Activation of PV$^+$, but not SST$^+$, interneurons in the dentate gyrus promotes survival of proliferative newborn progeny during early phases of adult hippocampal neurogenesis. (**a**) A schematic diagram of the experimental design. (**b-d**) Shown are sample confocal images of staining of EdU, DCX and DAPI of the dentate gyrus after the sham no-light treatment or 8 Hz light stimulation of ChR2$^+$PV$^+$ neurons (**b**). Scale bar: 50 μm. Also shown are summaries of stereological quantifications of total numbers of EdU$^+$ newborn progeny (**c**) and EdU$^+$DCX$^+$ newborn neuronal progeny (**d**) in the SGZ at 1 dpi before treatment and at 4 dpi after different treatments. Values represent mean ± s.e.m. (n = 3–5 animals; **: $P < 0.01$; *: $P < 0.05$; n.s.: $P > 0.1$; one-way ANOVA). (**e-g**) Activation of PV$^+$ neurons at 8 Hz reduces cell death of newborn progeny. Shown in (**e**) are sample confocal images of staining of Iba-1 (a microglia marker), EdU and DAPI. Note engulfing of EdU$^+$ and EdU$^-$ pyknotic nuclei by Iba-1$^+$ microglia. Scale bars: 10 μm. Also shown are percentages of EdU$^+$ cells that were surrounded by Iba-1$^+$ microglia (EdU$^+$Iba-1$^{\#}$; **f**) and total number of EdU$^-$ cells that were surrounded by Iba-1$^+$ microglia (EdU$^-$Iba-1$^{\#}$; **g**) at 4 dpi. Values represent mean ± s.e.m. (n = 4 animals; **: $P < 0.01$; Student's t-test).

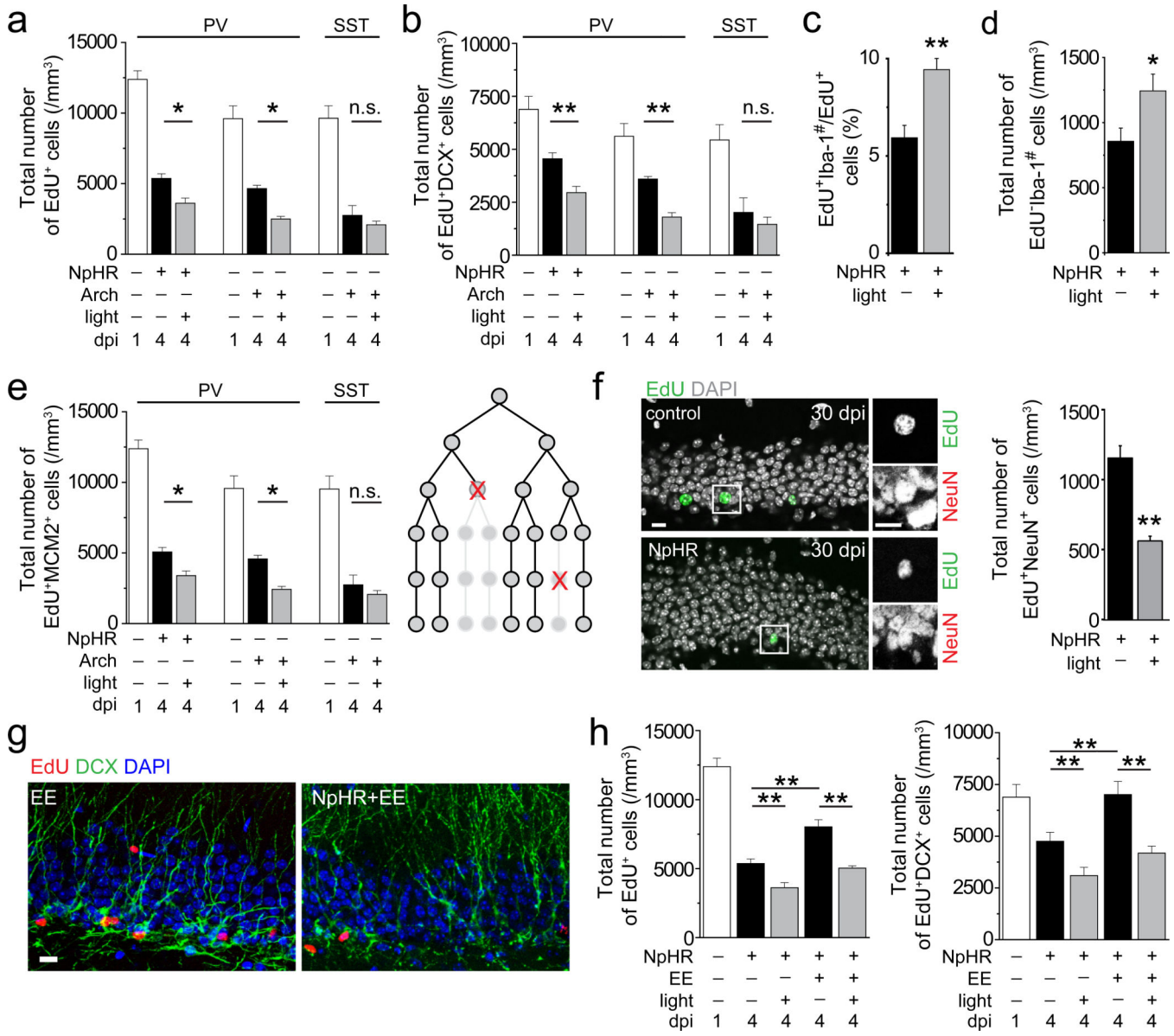

Figure 3.

Suppression of PV$^+$, but not SST$^+$, interneuron activity in the adult dentate gyrus decreases survival of newborn progeny in the normal and enriched environment. (**a-d**) The experimental paradigm is illustrated in Supplementary Fig. 7a and analyses were performed similarly as in Figs. 2c-d. Values represent mean ± s.e.m. (n = 3–5 animals; **: $P < 0.01$; *: $P < 0.05$; n.s.: $P > 0.1$; one-way ANOVA and Student's t-test). (e) Stereological quantifications of total numbers of EdU$^+$ cells that remained MCM$^+$, indicative of active proliferation, at 1 and 4 dpi. Values represent mean ± s.e.m. (n = 3–5 animals; **: $P < 0.01$; two-way ANOVA). As illustrated in a schematic diagram, death of a proliferating progenitor leads to elimination of all its progeny, thus potentially having a bigger impact on the final cell number compared to cell death of individual post-mitotic neurons. (**f**) Suppression of PV$^+$ neuron activity between 1 and 4 dpi leads to decreases in the final number of

EdU^+NeuN^+ adult-born neurons at 30 dpi. Shown are sample confocal images of staining of EdU, NeuN and DAPI at 30 dpi. Scale bar: 10 μm. Also shown is a summary of stereological quantification of EdU^+NeuN^+ cells at 30 dpi. Values represent mean ± s.e.m. (n = 3–4 animals; **: $P < 0.01$; Student's t-test). (**g**) Sample confocal images of staining of EdU, DCX, and DAPI in the adult dentate gyrus at 4 dpi with light stimulation or sham treatment, in normal or enriched environments between 1 and 4 dpi. Scale bar: 10 μm. (**h**) Summaries of stereological quantifications similar as in (**a-b**). The same data under the normal condition from (**a-b**) are re-plotted for comparison. Values represent mean ± s.e.m. (n = 3–5 animals; **: $P < 0.01$; two-way ANOVA and Student's t-test).